

# Intelligent cooperation management among solar powered base stations towards a green cellular network in a country with an equatorial climate

Mohammed H. Alsharif<sup>1</sup> · Rosdiadee Nordin<sup>1</sup> · Mahamod Ismail<sup>1</sup>

Published online: 12 June 2015  
© Springer Science+Business Media New York 2015

**Abstract** Energy efficiency in cellular networks is a growing concern for cellular operators with regard to maintaining profitability and reducing their overall environmental impact. Because evolved node Bs (eNBs) for long-term evolution wireless cellular networks are deployed to accommodate peak traffic, they are underutilized most of the time, especially under low-traffic conditions. Hence, switching eNBs on and off in accordance with traffic pattern variations is considered to be an effective method of improving energy efficiency in cellular networks. However, two main concerns of network operators when applying this technique are coverage issues and securing radio service for an entire area in response to the increased size of some cells to provide coverage for cell areas that are switched off. This study focuses on the parameters that affect coverage in order to find a balance between cellular network energy consumption and the area of cell coverage. To achieve this goal, particle swarm optimization, a bio-inspired computational method, has been adopted in this study to maximize the cell coverage area under the constraints of the transmission power of the eNB ( $P_{tx}$ ), the total antenna gain ( $G$ ), the bandwidth ( $BW$ ), the signal-to-interference-plus-noise ratio ( $SINR$ ), and shadow fading ( $\sigma$ ). In addition, the study investigated potential for gains in operational expenditures by operating eNB on solar energy. The

optimum criteria, including economic, technical and environmental feasibility parameters, were analyzed using the HOMER.

**Keywords** Energy efficiency · Green networks · Cellular base station cooperation · Mobile operators cooperative · Powered-on/off BSs · Solar base station

## 1 Introduction

The number of long term evolution (LTE) base stations (BSs) is expected to reach 2.43 million by 2018 to achieve a population coverage target of 1.3 billion LTE subscribers [1]. According to [2], BSs are considered to be the primary source of energy consumption in cellular networks and account for 57 % of the total energy used. Therefore, power reduction at BSs is the primary focus in creating green cellular networks. It is increasingly important for cellular operators to achieve energy efficiency in cellular networks to maintain profitability and reduce the overall environmental impact of these networks. According to [3], the emissions of carbon dioxide ( $CO_2$ ) are predicted to rise to 349 Mt $CO_2$  in 2020, with 51 % of emissions originating from the mobile sector, if this issue is not addressed. Thus, mobile operators are under immense pressure to meet both the demands of environmental conservation and cost reduction.

Recently, many research studies have been conducted to address this issue using ‘greener’ cellular networks that are less expensive to operate. Two approaches can be used to reduce environmental impacts and costs. In the first approach, power-efficient hardware is used to reduce BS power consumption. In the second approach, intelligent management of network elements is adopted based on traffic load varia-

✉ Mohammed H. Alsharif  
moh859@gmail.com

Rosdiadee Nordin  
adee@eng.ukm.my

Mahamod Ismail  
mahamod@eng.ukm.my

<sup>1</sup> Department of Electrical, Electronics and System Engineering, Faculty of Engineering and Built Environment, University Kebangsaan Malaysia, 43600 Bangi, Selangor, Malaysia

tions [4]. However, switching BSs off is considered to be an effective way to improve the energy efficiency for two reasons: (i) the key source of energy usage in cellular networks is the operation of BS equipment, and (ii) the infrastructures of cellular networks are designed to support daytime traffic. Traffic loads during the day differ from those at night. Hence, the amount of energy that is wasted because of the inefficient use of resources should not be overlooked, particularly for low and idle loads [5].

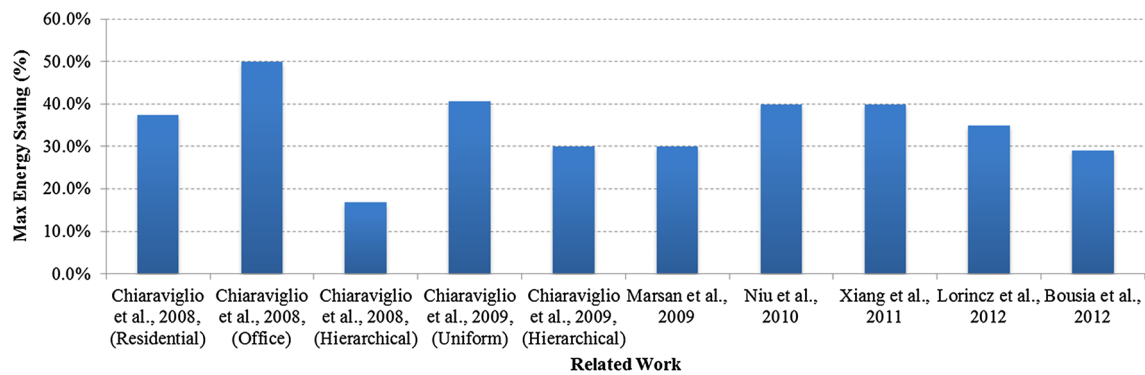
The philosophy behind the approach of reducing energy consumption based on traffic load is that if traffic is low in a given area, several cells can be switched off, and the radio coverage and service can be provided by the remaining active cells. However, two main concerns of network operators when applying this technique are coverage issues and securing radio service for an entire area in response to the increased size of some cells to provide coverage for cell areas that are switched off. Therefore, this study focuses on the parameters that affect coverage to find a balance between cellular network energy consumption and cell coverage area. To this end, particle swarm optimization (PSO) has been adopted in this study to maximize the cell coverage area under the constraints of transmission power of the BS ( $P_{Tx}$ ), total antenna gain ( $G$ ), bandwidth ( $BW$ ), signal-to-interference-plus-noise ratio ( $SINR$ ), and shadow fading ( $\sigma$ ). However, the electrical grid is the primary power source for BSs. The specific needs in the power supply for BS such as cost effectiveness, efficiency, sustainability and reliability can be met with technological advances in renewable energy. Moreover, there are numerous drivers and motivators for the deployment of renewable energy technologies and the transition towards green energy: this energy is free, clean, and abundant in most locations throughout the year. Hence, this study also investigates the potential for gains in OPEX by operating BSs on solar energy, where the optimum criteria, including economic, technical and environmental feasibility parameters, were analyzed using the hybrid optimization model for electric renewables (HOMER) software developed by the National Renewable Energy Laboratory (NREL).

The remainder of this paper is organized as follows: Sect. 2 includes related works. The cell switching scheme and cell coverage area optimization problems are described in Sect. 3. Section 4 presents a brief introduction of the considered PSO algorithm. The PSO simulation setup and optimization programming are provided in Sect. 5. The renewable energy approach and the potential for applying renewable energy for LTE-BS deployment in Malaysia are presented in Sect. 6. Section 7 describes the system architecture. Section 8 presents a brief introduction to the HOMER software, and Sect. 9 provides a HOMER simulation setup. Results and discussion are provided in Sect. 10, and Sect. 11 concludes the paper.

## 2 Related works

Several studies have investigated the switch-off approach. In [6–8], different approaches were presented for switching off a specific number of base stations BSs in Universal Mobile Telecommunications System (UMTS) cellular networks during low-traffic periods. A randomly chosen number of BSs was switched off, and the energy reduction was computed by simulating UMTS cellular networks [6]. The same authors have also presented an improvement of their previous work. They proposed a dynamic network planning scheme for switching BSs on and off and considered a uniform and hierarchical scenario [7]. In another study [8], demonstrated how to optimize energy savings by assuming that any fraction of cells can be switched off based on a deterministic traffic variation pattern over time. In addition, two approaches that achieve energy savings were proposed in [9]: (i) a greedy centralized algorithm, where each BS is examined based on its traffic load to determine if the BS will be switched off, and (ii) a decentralized algorithm, where each BS locally estimates its traffic load and independently decides if it is going to be switched off. Reference [10] proposed a dynamic switch on/off algorithm based on blocking probabilities. The BSs are switched off based on the traffic variation with respect to a blocking probability constraint. Reference [11] studied the optimal number of active BSs that will be deployed based on the trade-off between fixed power and dynamic power. Reference [12] presented a novel optimization model that can be used for energy-saving purposes at the level of a UMTS cellular access network. Reference [13] proposed a switch-off decision-making scheme based on the average distance between BSs and UEs, where the BS at the maximum average distance will be switched off.

In the literature, there are a number of studies that consider dynamic cell size adjustments to reduce energy consumption. Among them, Reference [14] introduced the cell zooming concept, which adaptively adjusts the size of the cells based on the current traffic load, to obtain energy savings. In their work, they used a cell zooming server, which is a virtual entity in the network controls, to manage the cell zooming procedure. The cell zooming server collects information, such as the traffic load, channel conditions, and user requirements, and subsequently determines if there are opportunities for cell zooming. The authors also proposed centralized and distributed versions of user association algorithms for cell zooming. Another study that considered variable cell sizes for energy savings is [15]. In this work, Bhaumik et al. considered two types of BSs: subsidiary BSs with a low transmission power and umbrella BSs with a high transmission power. They proposed a self-operating network that adaptively turns subsidiary and umbrella BSs on and off based on the current traffic demands. Similarly, Reference [16] assumed a cellular network consisting of micro- and macro-



**Fig. 1** Summary of previous studies that have investigated the potential for energy savings

BSs, where micro-BSs can be switched on and off, while macro-BSs can iteratively adjust their transmission power until the required QoS is achieved. They proposed static centralized, dynamic distributed, and hybrid topology management schemes to reduce the overall energy consumption of the network while satisfying certain QoS requirements. Figure 1 provides a summary of related works that have investigated the potential for reducing energy consumption via the switch-off approach.

The following are examples of the adoption of renewable energy resources such as solar and wind power in BSs. In India, efforts have been made to optimize the size of wind turbine generators (WTG), solar photovoltaic (SPV) arrays and other components for a hybrid power system; generator-based power supplies for global system for mobile communication (GSM, alternatively referred to as 2G) and code division multiple access (CDMA, 3G) standards have also been investigated [17, 18]. Reference [19] studied the feasibility of implementing an SPV/diesel hybrid power generation system suitable for a GSM base station site in Nigeria. Reference [20] discussed an SPV-Wind-Diesel-Battery system for a station in Catalonia, Spain. In Nepal, reference [21] studied the optimization of a Hybrid SPV/Wind Power System for a Remote Telecom Station. Kanzumba et al. [22] investigated the potential for using hybrid photovoltaic/wind renewable systems as primary sources of energy to supply mobile telephone base transceiver stations in the rural regions of the Republic of the Congo. Reference [23] discussed three types of renewable energy: (i) a SPV-battery system, (ii) SPV-fuel cell (FC) system and (iii) SPV-FC-battery system. The modelling and sizing optimization of such hybrid systems feeding a stand-alone DC load at a telecom base station has been implemented using the HOMER software. Vincent et al. [24] proposed a hybrid (Solar & Hydro) and DG system based on the power system models for powering stand-alone BS sites. Table 1 provides a summary of related works that have investigated green wireless network optimization strategies within smart grid environments.

### 3 Mechanism of proposed cell-switching scheme

This subsection presents an algorithm proposed for reduced energy consumption in cellular networks by reducing the number and size of active macro-cells based on traffic conditions. It is necessary to know the architecture of the BS as well as the power consumption by various BS parts, summarized in Table 2, with a  $2 \times 2$  MIMO configuration. More details on the BS internal components can be found in [25].

We start with a motivational example in Fig. 2 that shows a real traffic profile from a cellular wireless access network.

If the traffic load in a given area is low, several cells will be switched off, and the other cells will provide radio coverage and service for the entire region. The question that naturally arises is the following: which cells should be switched off, and which cells should remain active? How to determine which of the cells remain active depends on two factors. The first is the ease with which radio coverage can be provided to neighboring cells to guarantee service. The second is that the largest possible number of neighboring cells should be switched off to obtain the greatest decrease in energy requirements. The cells that satisfy these conditions are located in the middle of a cluster (called *master cells* in this study, indicated in Fig. 3 as yellow cells) and can easily provide coverage to neighboring cells that will be switched off later. Herein, two cases are discussed:

- (i) The normal case of a high traffic load ( $0.4 < \lambda \leq 1$ ): The network consists of 29 identical cells, which provide coverage to a 42.38 km<sup>2</sup> area, where each cell has an optimum radius of 750 m. The radius is chosen based on two considerations: (a) a small cell radius or small cell size, which results in a radio transmitters (BSs) and receivers (UEs) that are closer to each other and mitigates properties of the received signal, such as propagation path loss, multi-path fading, and shadow fading, which is due to higher SINR and spectral efficiency, and (b) the cost of the infrastructure of a wireless system, which is linearly proportional to the number of BSs. Therefore, the macro-

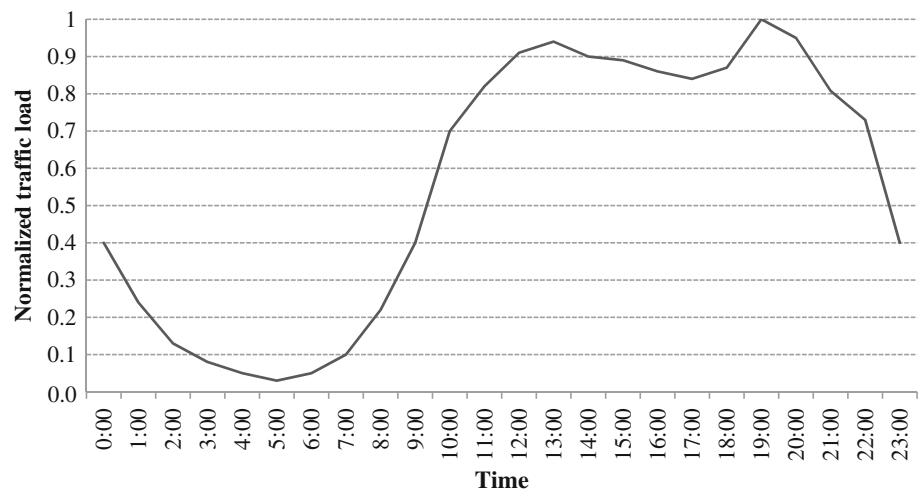
**Table 1** Summary of the techniques discussed

Year of publication	Renewable energy resource	Storage and support system	Cellular generation	Case study
2009 [23]	Photovoltaic	Battery	GSM	India
	Wind	Fuel-cell		
		Diesel generator		
2010 [18]	Photovoltaic	Battery	GSM	India
	Wind	Diesel generator	UMTS	
2012 [17]	Photovoltaic	Battery	GSM	India
	Wind	Polar DC generator	CDMA	
2012 [22]	Photovoltaic	Battery	GSM	Congo
	Wind	Diesel generator		
2013 [19]	Photovoltaic	Battery	GSM	Nigeria
		Diesel generator		
2013 [20]	Photovoltaic	Battery	GSM	Spain
	Wind	Diesel generator		
2013 [21]	Photovoltaic	Battery	GSM	Nepal
	Wind	Fuel-Cell	CDMA	
		Diesel generator		
2013 [24]	Photovoltaic	Battery	GSM	Nigeria
	Hydro turbine	Diesel generator		

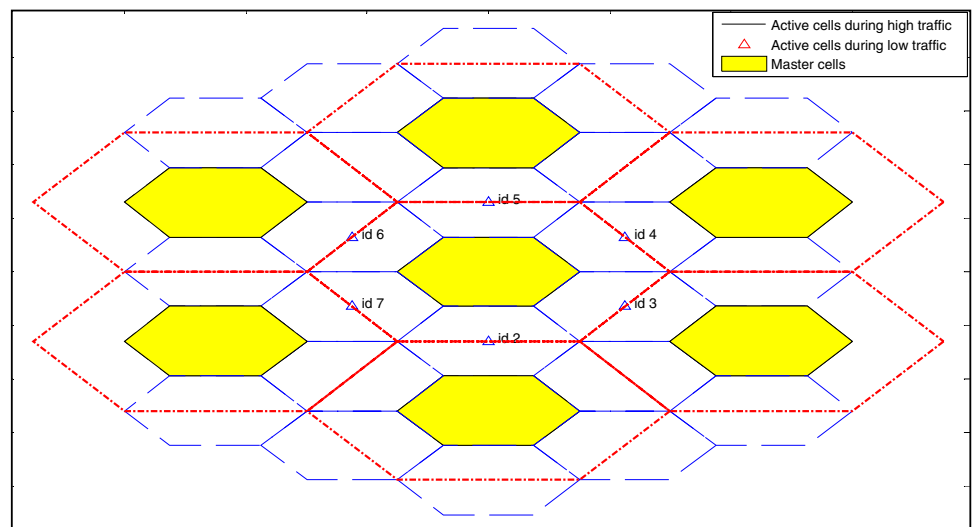
**Table 2** Power consumption of the hardware elements in LTE BS [25]

Item	Notation	Unit	Macro-BS
PA	Max transmit ( <i>rms</i> ) power	W	39.8
	Max transmit ( <i>rms</i> ) power	dBm	46.0
	PAPR	dB	8.0
	Peak output power	dBm	54.0
	PA efficiency, $\mu$	%	38.8
	Feeder loss, $\sigma$	dB	3.0
	<b>Total PA</b> ( $P_{PA}) = \frac{P_{max}}{\mu}$	W	<b>102.6</b>
TRX	$P_{TX}$	W	5.7
	$P_{RX}$	W	5.2
	<b>Total RF</b> ( $P_{RF}$ )	W	<b>10.9</b>
BB	Radio (inner <i>Rx/Tx</i> )	W	5.4
	Turbo code (outer <i>Rx/Tx</i> )	W	4.4
	Processor	W	5.0
	<b>Total BB</b> ( $P_{BB}$ )	W	<b>14.8</b>
DC-DC loss, $\sigma_{DC}$	%	6.0	
Cooling loss, $\sigma_{cool}$	%	9.0	
AC-DC (main supply) loss, $\sigma_{MS}$	%	7.0	
<b>Total per TRX</b> = $\frac{P_{PA} + P_{RF} + P_{BB}}{(1 - \sigma_{DC})(1 - \sigma_{cool})(1 - \sigma_{MS})}$	W	<b>160.8</b>	
Number of sectors	#	3	
Number of antennas	#	2	
Number of carriers	#	1	
Total number of transceivers ( $N_{TRX}$ )	#	6	
Total number of $N_{TRX}$ chains, $P_{in} = N_{TRX} \times \text{Total per TRX}$	W	<b>964.9</b>	

**Fig. 2** The daily traffic load pattern of the BS [2]



**Fig. 3** Cellular network structure (The blue cells represent a normal case with  $R_{org} = 750$  m, and the red cells represent low-traffic loads with  $R = 2R_{org} = 1.5$  km) (Color figure online)



cells yield the lowest cost for many scenarios because fewer BSs are used to provide coverage for a large area, indicating that coverage (i.e., the cell range) is an important parameter in designing wireless systems [26].

In this case, all cells in the network (29 cells) are active, and the BSs operate with full functionality to provide the full coverage needed to guarantee radio service, as shown in Fig. 3 for the cells framed in blue. However, this category of traffic continues for only 13 h (10 a.m. to 11 p.m.), as shown in Fig. 2. After this period, the mobile traffic decreases to under 0.4, which represents a low-traffic-load case. This is the focus of this study: we seek to achieve a balance between reducing energy consumption in the network and maximizing coverage to guarantee radio service and to achieve energy savings.

(ii) A low traffic load ( $0 < \lambda \leq 0.4$ ): It is well known that power consumption grows proportionally with the number of cells. In this case, the number of cells is reduced

by 75.86 % (22 cells will be switched off) by increasing the area coverage of the cells that are located in the middle of the cluster, i.e., the yellow *master cells* in Fig. 3, which provide coverage for the whole area. The following paragraph discusses the mechanism of the cell switching process.

During operation, the cells are monitoring the traffic load and are able to switch off when the traffic load drops and stays below a certain threshold for a certain period of time. At this time, the master cells inform their six neighboring BSs in the same cluster to prepare to switch off by sending a multicast control signal via an X2 signalling interface. Upon receipt of the switch-off control signal, neighboring cells immediately begin to decrease their transmission power gradually, and their resident UEs will inter-handover to a master cell based on a stronger UE-BS path. As the master cells monitor the traffic load when the traffic load increases, they send wake-up control messages via X2 signalling to the neighboring cells to signal these cells to return to operation. The neighboring cells



will begin gradually increasing their transmission power, and the resident UEs in the network will inter-handover to these cells based on a stronger UE-BS path.

Increasing the coverage area for master cells may lead to a lack of coverage, especially at the edge of the cell, due to the fact that the received signal power rapidly decreases as the transmit-receive distance increases; in addition, there is an increase in attenuation factors such as, shadowing fading, and multipath fading, among others. The following subsection will highlight the mathematical model and optimization formulation for a cell coverage area, taking into consideration the most important parameters in maintaining the best coverage at the edge of the cell.

### 3.1 Mathematical model and problem formulation

#### 3.1.1 Propagation model

The coverage depends on many parameters, the most important of which are the surrounding environment and the maximum radius of the cell, which have significant impacts on the received signal. However, three phenomena primarily affect the properties of the received signal: propagation path loss, multi-path (small-scale) fading, and shadow (large-scale) fading. The properties are modelled as a zero-mean Gaussian random variable with a variance on a logarithmic scale. Therefore, a basic propagation model for the received power ( $P_{rx}$ ) can be written as follows [27]:

$$P_{rx} = P_{tx} + G - L_{Hata} - \sigma, \quad \text{[dBm]} \quad (1)$$

where  $P_{tx}$  and  $G$  denote the transmitted power and the total antenna gain, respectively;  $L_{Hata}$  represents the Hata path loss model; and  $\sigma$  is the shadow fading margin.

The Hata path loss model is expressed as a function that includes the frequency ( $f$ ), BS antenna height ( $h_b$ ), UE antenna height ( $h_m$ ), and radius of the cell ( $R$ ). The basic formula for the Hata path loss is [27]

$$L_{Hata} = 69.55 + 26.16 \text{Log}_{10}(f_{MHz}) - 13.82 \text{Log}_{10}(h_b) - a(h_m) + [44.9 - 6.55 \text{Log}_{10}(h_b)] \times \text{Log}_{10}(R_{km}) - K_{suburban} \quad \text{[dB]} \quad (2)$$

$$a(h_m) = [1.1 \text{Log}_{10}(f_{MHz}) - 0.7] \times h_m - [1.56 \text{Log}_{10}(f_{MHz}) - 0.8] \quad (3)$$

$$K_{suburban} = 4.78 [\text{Log}_{10}(f_{MHz})]^2 - 18.33 \text{Log}_{10}(f_{MHz}) + 40.94. \quad (4)$$

The cell coverage area in a cellular system is defined as the percentage of the area within a cell that has received a signal at a power above a given minimum  $P_{min}$ . A cell requires some minimum received  $SINR$  for acceptable performance;

the  $SINR$  requirement translates to a minimum  $P_{min}$  throughout the cell. The transmission power at the base station is designed for an average amount of received power at the cell boundary of  $P_{min}$ . However, random shadowing and path loss will cause some locations within the cell to have a received power below  $P_{min}$ . According to [28], the minimum received power  $P_{min}$  can be expressed as follows,

$$P_{min} = N_o Bw + N_f + SINR + IM \quad \text{[dBm]} \quad (5)$$

where  $N_o Bw$  represents the thermal noise level for a specified noise bandwidth,  $N_f$  is the noise figure for the receiver, and  $IM$  is the implementation margin.

#### 3.1.2 Cell coverage and problem formulation

It is important that a balance between coverage and energy consumption be achieved for cellular green networks. The closed form for the cell coverage can be expressed as follows [29],

$$C = Q(a) + \exp\left(\frac{2-2ab}{b^2}\right) Q\left(\frac{2-ab}{b}\right) \quad [\%] \quad (6)$$

$$a = \left(\frac{P_{min} - P_{rx}(r)}{\sigma_\phi}\right), b = \left(\frac{10\alpha \log_{10}(\text{exp})}{\sigma_\phi}\right), \quad (7)$$

where  $\sigma_\phi$  is the standard deviation of the shadow fading and  $\alpha$  is a path loss exponent. In Eq. (6), the cell coverage area is expressed as a function  $C = f(a, b) = f(P_{min}, P_{rx}, \alpha, \sigma_\phi)$ , where the minimum received power is expressed as a function  $P_{min} = f(N_o, BW, N_f, SINR, IM)$  and the received power is  $P_{rx} = f(P_{tx}, G, L, \sigma)$ . The problem formulation is described as follows:

$$(p:) \quad \underset{P_{tx}, G, BW, SINR, \sigma}{\text{maximize}} \quad \left[ Q(a) + \exp\left(\frac{2-2ab}{b^2}\right) Q\left(\frac{2-ab}{b}\right) \right] \quad (8)$$

subject to the following constraints:

$$0 < P_{tx} \leq P_{tx}^{\max} \quad (9)$$

$$G_{\min} \leq G \leq G_{\max} \quad (10)$$

$$BW_{\min} \leq BW \leq BW_{\max} \quad (11)$$

$$SINR_{\min} \leq SINR \leq SINR_{\max} \quad (12)$$

$$\sigma_{\min} \leq \sigma \leq \sigma_{\max}. \quad (13)$$

It is clear that the problem posed by Eq. (8) is a nonlinear optimization problem. A PSO algorithm has been adopted to maximize coverage under the constraints  $P_{tx}$ ,  $G$ ,  $BW$ ,  $SINR$ , and  $\sigma$ . This algorithm has several advantages, such as lower computational costs, better performance, and fewer

**Table 3** List of simulation parameters

Item	Parameter	Acronym	Value	Unit
Network parameters	Carrier frequency	$f_c$	2.6	GHz
	LTE bandwidth	$BW$	1.4–20	MHz
	Max. cell radius	$R$	1.5	km
	Max. number of cells	$cell$	29	#
Base station parameters	Max. BS transmission power	$P_{tx}^{max}$	46	dBm
	BS antenna height	$h_b$	10	m
	Tx antenna gain	$G$	5–15	dB
	Number of antenna	$N_{ant}$	2	#
	Max. total power consumption	$P_{max\_tot}^{BS}$	965	W
Mobile station parameters	Thermal noise density	$N_o$	174	dBm/Hz
	Noise figure	$N_f$	9	dB
	Implementation margin	$IM$	3	dB
	UE antenna height	$h_m$	1.5	m
Propagation losses	Morphology	Suburban		
	Propagation model	Hata path loss model		
	SINR	$SINR_{min}$	-5.1	dB
		$SINR_{max}$	18.6	
	Shadow fading margin	$\sigma$	4–8	dB
	Exponent path loss	$\alpha$	3.7	#
Standard deviation of the shadow	$\sigma_\phi$	4	dB	

adjustable parameters, compared to other global optimization algorithms [30].

#### 4 Bio-inspired particle swarm optimization algorithm

The PSO algorithm was proposed by Kennedy and Eberhart in 1995 [30]. A PSO is initialized using a group of randomly positioned particles, and it subsequently searches for an optimal point; the position and velocity of each particle in the swarm, with  $N$  decision parameters in the optimization problem, are defined as  $X_i = (x_{i1}, x_{i2}, \dots, x_{in})$  and  $V_i = (v_{i1}, v_{i2}, \dots, v_{in})$ , respectively. The best previous position of each particle is defined as  $P_i = (p_{i1}, p_{i2}, \dots, p_{in})$ , and the global best position of all particles is represented by  $P_g = (p_{g1}, p_{g2}, \dots, p_{gn})$ . Therefore, the velocity and position of each particle are updated as follows:

$$v_{new} = w \times v_{old} + c_1 \times r_1 (p_{in} - x_{in}) + c_2 \times r_2 (p_{gn} - x_{in}), \quad (14)$$

where  $w$  is the inertia weight;  $r_1$  and  $r_2$  are random numbers, which are usually chosen between  $[0, 1]$ ;  $c_1$  is the self-recognition component coefficient, which is a positive constant;  $c_2$  is the social component coefficient, which is a positive constant; and the values  $c_1 = c_2 = 2$  are generally referred to as the learning factors. The following weighting function is usually utilized in Eq. (14):

$$w = \frac{w_{max} - [(w_{max} - w_{min}) \times iter]}{iter_{max}}, \quad (15)$$

where  $w_{max}$  is the initial weight, usually chosen as a large value less than 1;  $w_{min}$  is the final weight;  $iter$  is the current iteration number; and  $iter_{max}$  is the maximum iteration number. A large  $w$  enables a global search, whereas a small  $w$  enables a local search. Linearly decreasing the inertia weight from a relatively large value to a small value through the course of the PSO run gives the best PSO performance comparisons with fixed inertia weight settings.

From Eq. (14), a particle decides where to move next, considering its own experience, i.e., the memory of its best past position, and the experience of the most successful particle in the swarm. The new position is then determined using the previous position and the new velocity and can be written as,

$$x_{in\_new} = x_{in\_old} + v_{new}. \quad (16)$$

#### 5 Simulation setup and optimization programming

The simulation model has been implemented in MATLAB. Table 3 summarizes the simulation parameters.

The model applied in this study is described as follows in Fig. 4. In addition, the pseudocode of the PSO algorithm is shown in Fig. 5.

**Fig. 4** Model of maximized coverage programming

<b>Inputs</b>	<ul style="list-style-type: none"> <li>• Initialize network parameters (<math>f_c, h_b, h_m, N_o, N_f, \alpha, \sigma_\phi, IM</math>).</li> <li>• Initialize PSO parameters, Number of particles (<math>N= 20</math>), Learning factors (<math>c_1= c_2= 2</math>), Dimension of particles (<math>D= 5</math>), Stopping condition (<math>Iter. = 50</math>), Initial weight (<math>w_{max}= 0.9</math>), &amp; Final weight (<math>w_{min}= 0.4</math>).</li> </ul>
<b>Constraints</b>	<ul style="list-style-type: none"> <li>• <math>SINR_{min}= -5.1, SINR_{max}= 18.6; BW_{min}= 1.4, BW_{max}= 20; G_{min}= 5, G_{max}= 15; \sigma_{min}= 4, \sigma_{max}= 8; P_{tx,max}= 46</math> dBm.</li> </ul>
<b>Main algorithm</b>	<ul style="list-style-type: none"> <li>• Finding the best optimized coverage under the constraints of <math>P_{tx}, G, BW, SINR</math>, and <math>\sigma</math>.</li> </ul>
<b>Outputs</b>	<ul style="list-style-type: none"> <li>• Given optimal solution best global fitness (<i>Max. coverage</i>) and the best global position (<math>P_{tx}, G, BW, SINR</math>, and <math>\sigma</math>).</li> </ul>

### 6 Potential of renewable energy for LTE-BS deployment in Malaysia

Malaysia lies entirely within the equatorial region between latitudes 1° and 7° North and longitudes 100° and 120° East [31], which offers an abundant potential for using renewable energy resources, such as solar and wind energy [32].

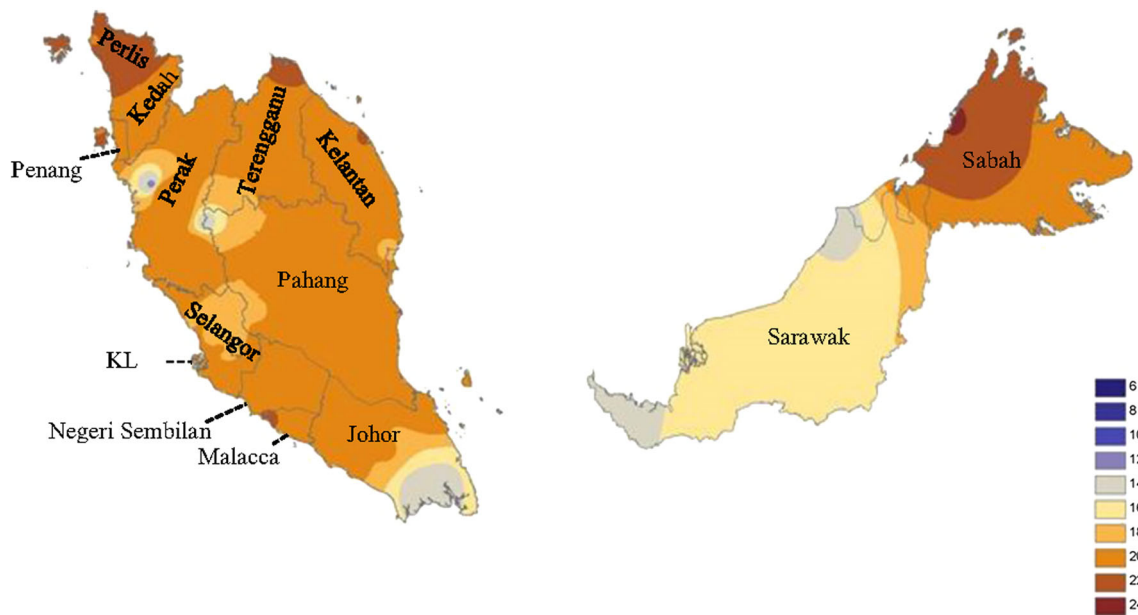
In the early 1980s, a study on Malaysia’s wind energy was conducted at the University Kebangsaan Malaysia (UKM). The Solar Energy Research Group from UKM collected wind data from 10 stations across the country for the period from 1982 to 1991. The data studied include hourly wind speed at the stations, mostly located at airports and near coasts, where land and sea breezes may influence the wind [33]. The study showed that the mean wind speed is low and not greater than 2 m/s. However, the wind does not blow uniformly and varies according to the month and region. The locations with the greatest wind power potential are Mersing and Kuala Terengganu, which are located on the East Coast of Peninsular Malaysia [32]. In 2014, reference [34] presented a study on predicting the wind speed in those states over the long term (23 years) using neural networks and a set of recent wind speed measurement samples from the two meteorological stations in those states. The results showed the mean wind speed to be low, not greater than 3.8 m/s.

As for solar energy, Malaysia has a stable climate throughout the year. Hence, the solar radiation in Malaysia is relatively high based on global standards. It is estimated that Malaysia’s solar power is four times that of the global fossil fuel resources [35]. The global irradiation fluctuates in the range of 2–6 kWh/(m<sup>2</sup> day). There is more cloud cover in the second part of the year (October to February) and, consequently, poorer solar potential compared with the first part of the year (March to October); the average temperature per day ranges from 33 °C during the day to 23 °C at night [36]. Moreover, the solar cells have low maintenance and high reliability, with a life span expectation of 20–30 years. In addition, it is estimated that one square meter of solar panel in Malaysia can result in an annual reduction of 40 kg of CO<sub>2</sub> [32], which makes solar power a favorable source of energy to be used in telecommunication applications in the future.

<b>Algorithm of the proposed scheme</b>	
1:	Initialize PSO parameters, Number of particles ( $N= 20$ ), Learning factors ( $c_1= c_2= 2$ ), Dimension of particles ( $D= 5$ ), Stopping condition ( $Iter. = 50$ ), Initial weight ( $w_{max}= 0.9$ ), & Final weight ( $w_{min}= 0.4$ ).
2:	Initial populations of particles $X_i = (P_{tx}, G, BW, SINR, \sigma)$ with random positions and zero velocities $V_i$ .
3:	Comparing the position of each particle with constraints
4:	<b>if</b> ( $X_i >$ max. constraints) <b>then</b>
5:	$X_i =$ max. constraints
6:	<b>end if</b>
7:	<b>if</b> ( $X_i <$ min. constraints) <b>then</b>
8:	$X_i =$ min. constraints
9:	<b>end if</b>
10:	Evaluate the initial fitness values $f(X_i)$ of each particle according to Eq. (8),
11:	Store the best initial fitness value and both of Pbest ( $P_i$ ) and Gbest ( $P_g$ ).
12:	<b>while</b> $i <$ iter <b>do</b>
13:	$r_1 = \text{rand} (); r_2 = \text{rand} ();$
14:	Calculate $w$ according to Eq. (15),
15:	Update $V_i$ according to Eq. (14),
16:	Update $X_i$ according to Eq. (16),
17:	Comparing the position of each particle with constraints
18:	Repeat steps 3 – 9
19:	Evaluate a new fitness values $f(X_i)$ of each particle
20:	Compare each particle's fitness evaluation with the current particle's to obtain the individual best position
21:	Compare fitness evaluation with the population's overall previous best to obtain the global best position
22:	<b>end while</b>
23:	Given optimal solution best global fitness ( <i>Max. coverage</i> ) and the best global position ( $P_{tx}, G, BW, SINR, \sigma$ ).

**Fig. 5** Pseudocode of the considered PSO algorithm





**Fig. 6** Annual average solar radiation [ $\text{MJ}/(\text{m}^2 \text{ day})$ ] (note that to convert  $\text{MJ}/(\text{m}^2 \text{ day})$  to  $\text{kWh}/(\text{m}^2 \text{ day})$ , it should be divided by 3.6) [31]

### 6.1 Solar energy

Solar radiation data in Malaysia have been the subject of earlier studies. Malaysia's climatic conditions are desirable for extending the utilization of SPV systems due to the high amount of solar radiation received throughout the year. The north region and a few areas in east Malaysia receive the highest amount of solar radiation throughout the year. Kuching has the lowest irradiance value, whereas Kota Kinabalu has the highest measured solar radiation [31]. Figure 6 provides information on solar radiation in different states of Malaysia.

It can be seen from Fig. 6 that Sabah, Perlis, and Kedah have sufficient solar resources to support solar energy applications. Figure 7 represents the daily solar radiation in these three states [32].

It can be seen that the average amount of daily solar radiation in Kedah, Sabah, and Perlis is  $5.48$ ,  $5.31$ , and  $5.24$   $\text{kWh}/\text{m}^2$ , respectively. The average solar radiation of these states reveals the high potential of the states to use SPV systems. Moreover, Fig. 8 shows Malaysia's average daily solar radiation, estimated to be  $5.15$   $\text{kWh}/(\text{m}^2 \text{ day})$  [32].

This study investigates five categories of average daily solar radiation  $5.1$ ,  $5.2$ ,  $5.3$ ,  $5.4$ , and  $5.5$   $\text{kWh}/\text{m}^2$ , to cover all the states as much as possible.

### 6.2 Hindrances to using SPV panels: progress and recommendations

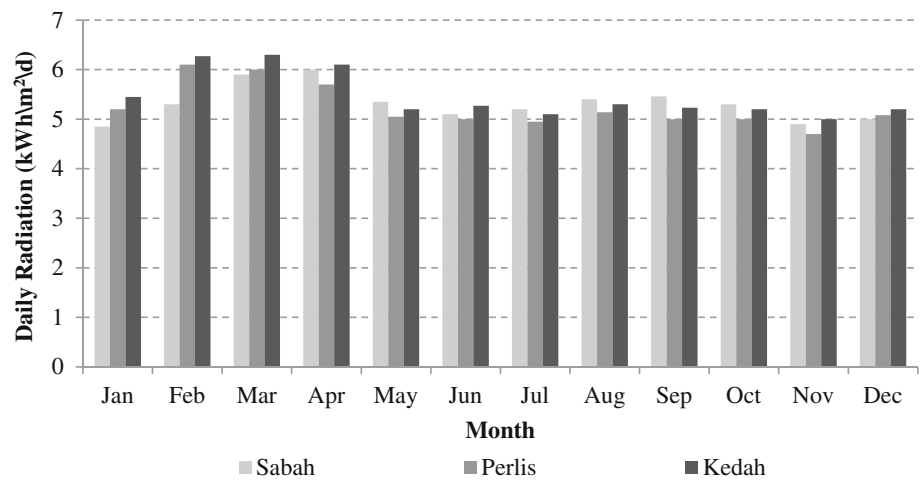
It is clear from the above discussion that Malaysia has abundant potential for using solar energy. Some barriers that affect

the performance of SPV panels should be taken into consideration because power shortages are not acceptable in the cellular network sector. The following section highlights these barriers.

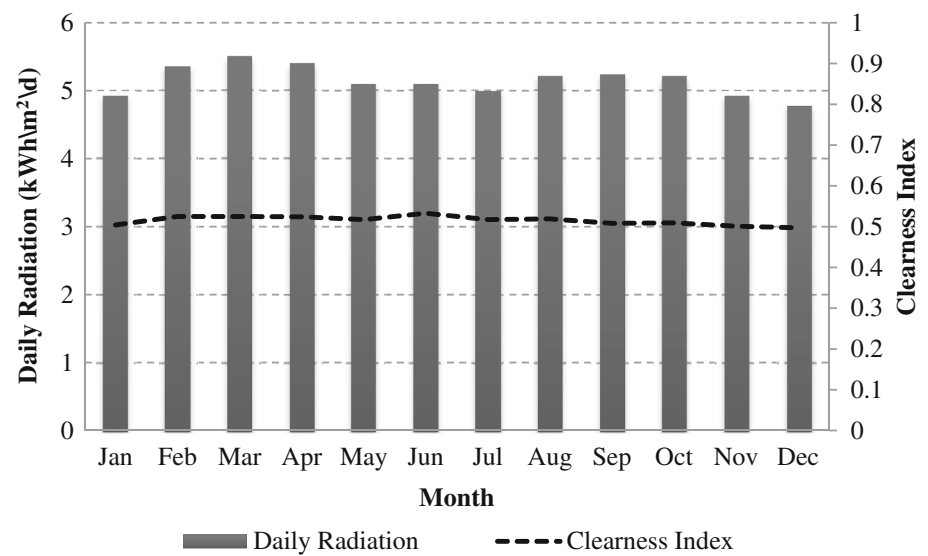
Radiation is higher than average in urban areas due to man-made structures and effects such as the reflection from the glass on buildings, which increases radiation. At the same time, the shade from tall buildings may dramatically reduce the power produced by solar cells during periods when the sunlight is blocked. However, Sabah, Perlis and Kedah have a low level of urbanization, with few tall buildings compared to the capital and surrounding states. On the other hand, the climate in the tropics during some seasons includes heavy rain and cloudy skies for several days at a time, causing battery banks to run out of charge sooner. To solve this problem, the study suggests the hybridization of the solar power system with the existing electrical grid, which will provide sustainability and reliability of the power supply to BS, especially given the short lifespan of the battery.

The dirt, dust, tree debris, moss, sap, water spots, and mold that develop on solar panels have a significant impact on the performance of solar power systems. Cleaning the panels is a challenge because the height necessary for SPV panels for good access to the sunlight makes them difficult to reach, so the rapid growth of moss and grass on the panels creates an extra cleaning cost for the owner of the panels. The dual-axis tracking system for the SPV array allows for wind, rain, and gravity to remove most debris and dust naturally. Moreover, surveillance and maintenance of the solar panels can be conducted by just two trained people.

**Fig. 7** Average daily radiation [kWh/(m<sup>2</sup> day)]



**Fig. 8** Malaysia’s average received daily solar energy



### 7 System architecture

Figure 9 is a schematic showing two subsystems, the BS and the renewable energy source subsystem.

The main components of a SPV power system are listed below:

1. *Solar panels* responsible for collecting sunlight and converting it into Direct Current (DC) power electricity. The SPV generator contains modules that are composed of many interconnected solar cells in a parallel series to form a solar array. The energy generated from the PV generator is represented by the following equation [22]:

$$E_{PV} = A \times \eta_m \times P_f \times \eta_{PC} \times I \tag{17}$$

where  $A$  is the total area of the photovoltaic generator (m<sup>2</sup>),  $\eta_m$  is the module efficiency (0.111),  $P_f$  is the packing factor (0.9),  $\eta_{PC}$  is the power conditioning efficiency (0.86), and  $I$  is the hourly irradiance (kWh/m<sup>2</sup>).

2. *Batteries bank* stores excess electricity for future consumption by the BS during night time, load-shedding hours, or if solar energy is not sufficient to feed the BS load completely. To protect the battery, the addition of a charge controller is recommended. A charge controller or battery regulator limits the rate at which electric current is added to or drawn from electric batteries. It prevents overcharging and may protect against overvoltage, which can reduce battery performance or lifespan and may pose a safety risk. It may also prevent completely draining (“deep discharging”) a battery or may perform controlled discharges, depending on the battery technology, to protect battery life [37].

The battery is modeled based on the state of charge (SOC) condition. The SOC of charging and discharging of the battery can be calculated from Eqs. (18) and (19), respectively [21], where  $\mu_{bat}$  is equal to the round-trip efficiency in the charging process,  $U_{nom}$  is the nominal DC voltage of individual battery,  $\Delta t$  is the hourly time step and is equal to a 1-h

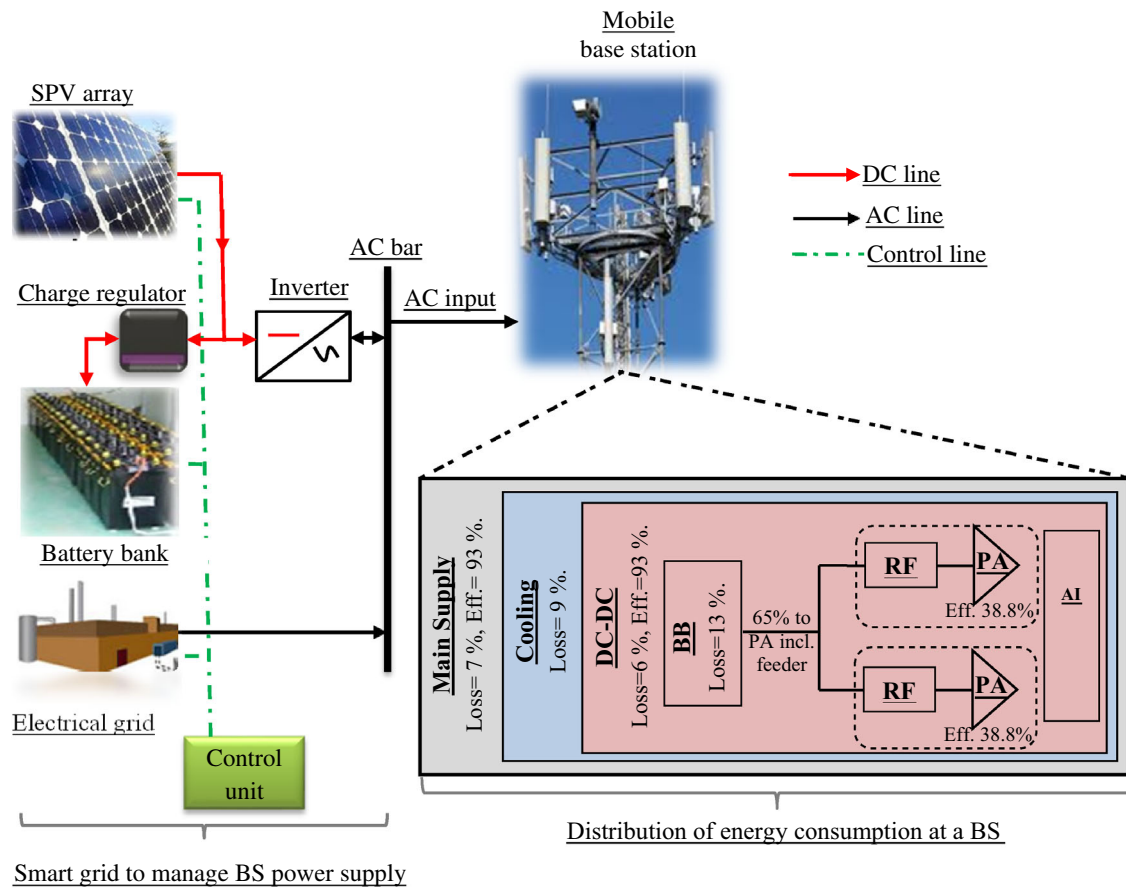


Fig. 9 System model of an adaptive power management scheme for an LTE- BS powered by a smart grid

interval,  $P_L$  is the BS power load, and  $P_S$  is the total power supplied to these stations.

$$Soc(t + 1) = Soc(t) + \eta_{bat} \left( \frac{P_S(t) - P_L(t)}{U_{nom}} \right) \Delta t \quad (18)$$

$$Soc(t + 1) = Soc(t) - \eta_{bat} \left( \frac{P_S(t) - P_L(t)}{U_{nom}} \right) \Delta t \quad (19)$$

The nominal capacity of the battery bank,  $C_N$ , is the maximum state of charge  $SOC_{max}$  of the battery and is represented by Eq. (20), where  $N_B$  is the total number of batteries,  $N_{BS}$  is the number of batteries connected in series, and  $C_B$  is the capacity of the battery.

$$C_N = \frac{N_B}{N_{BS}} C_B \quad (20)$$

The minimum state of charge of the battery,  $SOC_{min}$ , is set to its lower limit, which does not discharge below the minimum state of charge and is expressed in Eq. (21), where  $DOD$  is the depth of discharge of battery and  $SOC_{max}$  is the maximum state of charge [21].

$$SOC_{min} = (1 - DOD) \quad (21)$$

3. *Inverter* The main load (BS) depends on uninterruptible AC power. Therefore, a highly efficient inverter is required, which converts the DC voltage from the load busbar and battery to the requested AC-voltage. The inverter is also able to log information such as system performance (e.g., electricity produced by the system based on a daily, monthly or yearly basis) and safety measures to avoid electrical mishaps [37]. The efficiency of the inverter can be defined by the following equation:

$$\eta_{inv} = \frac{P}{P + P_0 + K P^2} \quad (22)$$

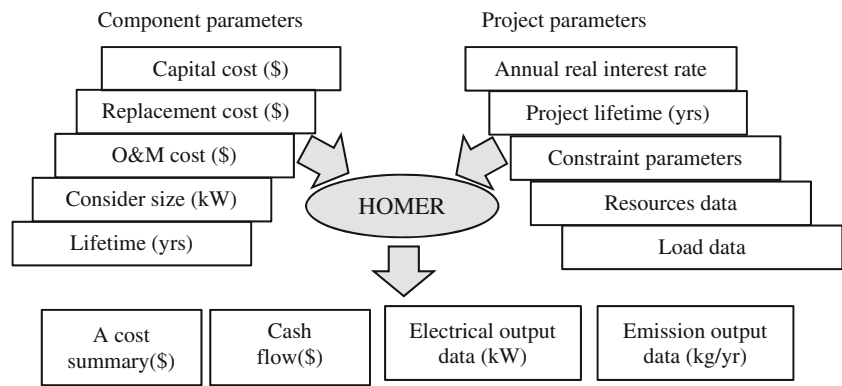
In which,  $P$ ,  $P_0$  and  $k$  can be determined using the following equations:

$$P_0 = 1 - 99 \frac{10}{\eta_{10}} - \frac{1}{\eta_{100}} - 9, \quad (23)$$

$$K = \frac{1}{\eta_{100}} - P_0 - 1, \quad (24)$$

$$P = \frac{P_{out}}{P_n} \quad (25)$$

**Fig. 10** Architecture of HOMER software



$\mu_{10}$  and  $\mu_{100}$  are provided by the manufacturers and represent the efficiency of the inverter at 10 and 100 %, respectively, of its nominal power. The efficiency of the inverter is roughly assumed to be constant over the whole of the working range (e.g., 90 %) [38].

4. **Control system** The control system of the power system is the brain of a complex control, regulation and communication system. For the remote interface, wireless modems or network solutions are the most common communication units. In addition to the control functions, data-logger and alarm memory capabilities are of great importance. All power sources work in parallel and are managed by a sophisticated control system and central control unit and share the load.

The optimum criteria, including economic, technical and environmental feasibility parameters, were analyzed using the HOMER software.

## 8 HOMER software hybrid power system modeling tool

HOMER [39] is primarily an optimization software package and simulates varied renewable energy sources (RES) system configurations and scales them based on the net present cost (NPC). NPC represents the life cycle cost of the system. The calculation assesses all costs that occur within the project lifetime, including initial set-up costs (IC), component replacements within the project lifetime and maintenance. Figure 10 presents the architecture of HOMER software.

HOMER calculates NPC according to the following equation:

$$NPC = \frac{TAC}{CRF} \quad (26)$$

where  $TAC$  is the total annualized cost (\$). The capital recovery factor (CRF) is represented by

$$CRF = \frac{i(1+i)^n}{(1+i)^n - 1} \quad (27)$$

where  $n$  is the number of years and  $i$  is the annual real interest rate (6 % in this case). HOMER assumes that all prices escalate at the same rate and applies an annual real interest rate rather than a nominal interest rate. NPC estimation in HOMER also considers the salvage cost, which is the residual value of the power system components at the end of the project lifetime. The equation to calculate salvage value ( $S$ ) is

$$S = rep \left( \frac{rem}{comp} \right) \quad (28)$$

where  $rep$  is the replacement cost of the component,  $rem$  is the remaining life of the component, and  $comp$  is the lifetime of the component. Annual savings are estimated by subtracting the annualized costs for each supply method from each other, providing the overall savings or loss for each year.

## 9 HOMER simulation configuration

The lifetime of the project is 20 years, and the annual real interest rate is assumed to be 6 %. HOMER makes a decision at each time step to meet the power needs at the lowest cost, subject to the constraint from the dispatch strategy chosen in the simulation and a set value of 80 %. The system must supply electricity to both the load (base station system) and backup power system every hour. In this study, the backup power is reserved by taking 10 % from the hourly load, to create enough spare capacity to serve the load, even if the hourly renewable energy output was to suddenly decrease by 10 %. Moreover, several sets of sizes will be considered in the simulation, taking into account the SPV, inverter and the number of batteries that will be used to achieve cost effectiveness, reliability, and efficiency in the optimization process. The efficiency of the inverter is roughly assumed to be constant over the working range (e.g., 90 %, based on a study from [38]), and the battery is set at 85 % [38]. For more

**Table 4** Simulation setup of the SPV/electric grid hybrid system

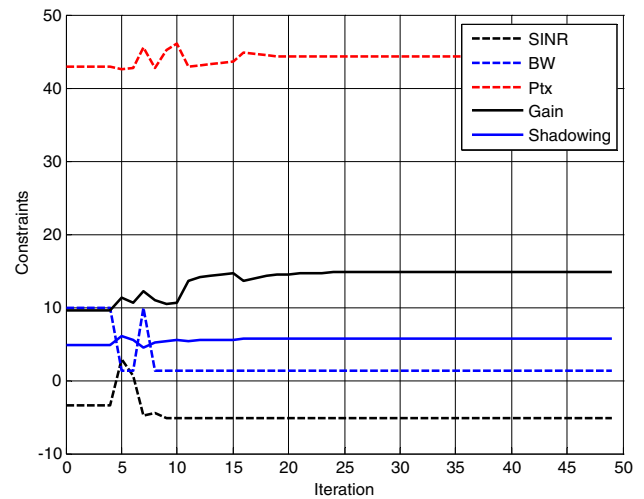
System components	Parameters	Value
Control parameters	Annual real interest rate	6 %
	Project lifetime	20 years
	Dispatch strategy	Cyclic charging
	Apply set point state of charge	80 %
	Operating reserve: as percent of load, hourly load	10 %
SPV	Sizes considered	1, 1.5, 2, 2.5 kW
	Operational lifetime	20 years
	Capital cost	\$4/W
	Replacement cost	\$4/W
	O&M cost/year	\$0.01/W
Inverter	Sizes considered	0.5, 1, 1.5, 2 kW
	Efficiency	90 %
	Operational lifetime	15 years
	Capital cost	\$0.9/W
	Replacement cost	\$0.9/W
Battery	O&M cost/year	\$0.01/W
	Number of batteries	5, 10, 11,12, 13, 14
	Round trip efficiency	85 %
	Minimum state of charge	30 %
	Nominal voltage	6 V
	Nominal current	360 Ah at the 20 h
	Nominal capacity	2.16 kWh
	Lifetime throughput	1075 kWh
	Max. charge rate	1 A/Ah
	Max. charge current	18 A
	Self-discharge rate	0.1 %/h
	Operational lifetime	8 years
	Capital cost	\$300
	Replacement cost	\$300
	O&M cost/year	\$10
Grid	Purchase capacity	0.8 kW
	Energy price	\$0.13/kWh

details on the the technical specifications, costs, economic parameters and system constraints that are used in this study, see Table 4 below.

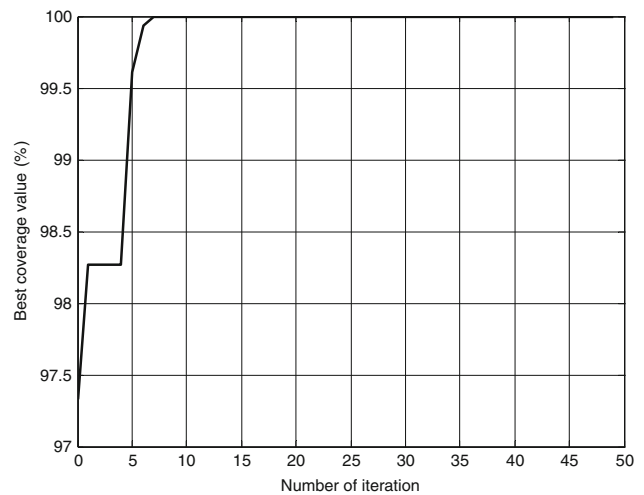
## 10 Results and discussion

### 10.1 Cell switching scheme

The PSO has been used to maximize coverage under five different constraints: (i) the transmission power of the eNB ( $P_{tx}$ ), (ii) the total antenna gain ( $G$ ), (iii)  $BW$ , (iv) the  $SINR$ ,



**Fig. 11** The behavior of constraint parameters that impact the cell coverage area



**Fig. 12** The behavior of the fitness function-coverage with change in the constraint parameters

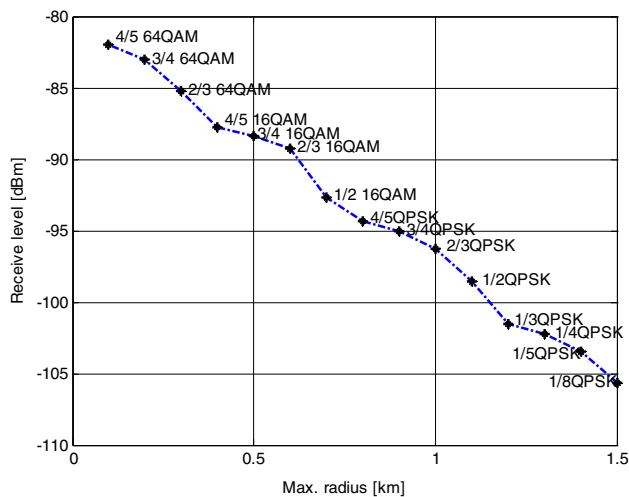
and (v) shadow fading ( $\sigma$ ). The impact of these parameters on the coverage is shown in Fig. 11.

The most important parameters for maintaining coverage at the edge of the cell, where the  $SINR$  is low and where the shadowing is high, are  $P_{tx}$  and  $G$ . When these parameters increase, the coverage also increases, as shown in Fig. 12.

The optimal transmission power  $P_{tx}$  and the antenna gain  $G$  achieved a maximum coverage at a maximum radius of 1.5 km, where the  $SINR$  was the lowest, at  $-5.1$  dB, and the shadowing, at 5.8 dB, is 44.24 dBm and 14.7 dB. Because the  $BW$  is proportional to the noise power, the optimum  $BW$  at the edge is 1.4 MHz.

For the downlink data transmissions in an LTE network, the eNB typically selects the modulation and coding scheme (MCS) based on the channel quality indicator (CQI) feedback characteristics of the UE's receiver, i.e., the  $SINR$  via a link



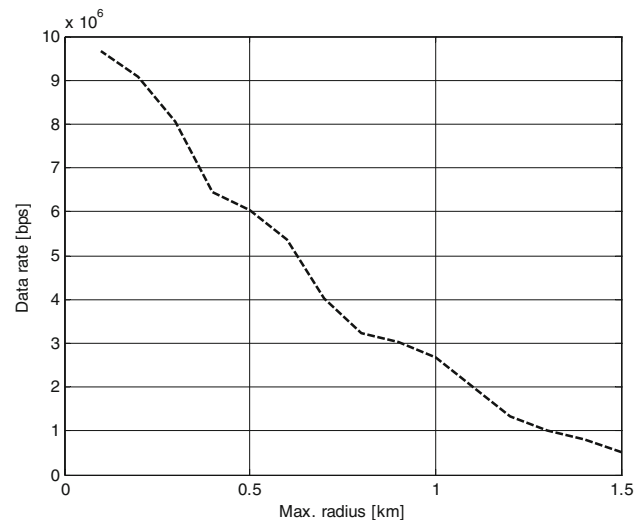


**Fig. 13** Cell radii versus receiver sensitivity power for different MCSs, with  $P_{rx} = 44.3$  dB<sub>m</sub> and  $BW = 1.4$  MHz

adaptation procedure. The SINR requirement translates into a minimum received power  $P_{min}$  throughout the cell. Figure 13 shows the relation, based on assumptions made in a reference [28], between the radius of the cell,  $P_{min}$  and the MCS.

It is clear that when the  $P_{min}$  decreases, the MCS decreases because the demodulation error rate increases as a result of the increase in both the noise and the interference that often occurs at the edge of a cell. Low-order modulation, such as quadrature phase shift keying (QPSK), is more robust and can tolerate higher levels of interference but provides a lower transmission bit rate, whereas the high-order modulation 64-QAM offers a higher bit rate but is more susceptible to errors because of its higher sensitivity to interference, noise and channel estimation errors. Therefore, the high-order modulation 64-QAM is only useful for a sufficiently high SINR. However, the bit rate and data rate depend on the MCS, BW, and the number of antennas. For any system, the data rate is calculated in symbols per second. Furthermore, it is converted into bits per second based on the how many bits a symbol can carry, which is dependent on the MCS. It is known that increasing the radius can cause the data rate to decrease because of the low SINR, high path loss, and low MCS level. Figure 14 highlights the data rate versus macro-cell radii, with  $P_{rx} = 44.3$  dBm and  $BW = 1.4$  MHz.

This study focuses on a cell radius of 1.5 km, which corresponds to that of a cell in a low-traffic case; the lowest modulation rate (QPSK) supports a 1.5-km cell radius. For LTE with a 1.4 MHz BW, this means that there are six resource blocks (RBs), each RB has 12 subcarriers, each subcarrier has seven symbols for normal CP, and the time of the slot is 0.5 ms. Hence, the total number of symbols per RB is  $12 \times 7 \times 2 = 168$  symbols/ms; therefore, there are 1008 symbols/ms. When 1/8 QPSK is used (2 bits/symbol), the data rate will be 252 Kbps for a single chain, and with  $2 \times 2$



**Fig. 14** Data rate versus macro-cell radii, with  $P_{rx} = 44.3$  dBm and  $BW = 1.4$  MHz

MIMO, the data rate will be two times that of a single chain, i.e., 504 Kbps.

## 10.2 Optimal design of the energy source hybrid SPV/electric grid system

For a high-traffic-load scenario, all cells (29 cells, from Fig. 3) in the network are active, and the BSs will work with full functionality to provide full coverage as needed to guarantee radio service. This level of traffic load continues for only 13 h (10 a.m. to 11 p.m.), as shown in Fig. 2. However, in the case of a low-traffic load, 22 cells will be switched off, while only seven cells, the ‘master cells’, will remain active. The ‘master cells’ operate for 24 h (13 h during high-traffic loads and 11 h during low-traffic loads) to provide coverage for the entire region. Therefore, this study investigated two designs of a hybrid power system. The first, for the cells that operate in high traffic, translates to only 22 cells, as shown with a blue frame in Fig. 3. The second, for the cells that operate 24 h, translates to seven cells, which are called master cells, as shown in Fig. 3, filled in yellow.

A different set of values of average daily solar radiation, 5.1, 5.2, 5.3, 5.4, and 5.5 kWh/m<sup>2</sup>, were taken into account in order to simulate the potential for the application of solar energy in a wide range of states. The total power consumption by the BS is 965 kW (as shown in Table 1), and the energy retail price is \$0.13/kWh [40]; in addition, this study assumes that the grid purchase capacity is fixed at 0.8 kW for all cases of solar radiation, based on that assumption the technical criteria was determined for an optimal design of the hybrid SPV/electric grid system. The energy output, the economic analysis of the proposed hybrid systems and the related sensitivity analysis are provided in the following paragraphs.































Solar (kWh/m <sup>2</sup> /d)						PV (kW)	L16P	Conv. (kW)	Grid (kW)	Initial Capital	Operating Cost (\$/yr)	Total NPC	COE (\$/kWh)	Ren. Frac.	Batt. Lf. (yr)
5.100						2.0	11	1.0	0.8	\$ 12,200	987	\$ 23,520	0.242	0.40	9.7
5.200						2.0	10	1.0	0.8	\$ 11,900	989	\$ 23,243	0.239	0.40	8.9
5.300						2.0	10	1.0	0.8	\$ 11,900	982	\$ 23,169	0.239	0.41	8.9
5.400						1.8	11	1.0	0.8	\$ 11,400	990	\$ 22,756	0.234	0.40	9.7
5.500						1.8	11	1.0	0.8	\$ 11,400	982	\$ 22,662	0.233	0.40	9.8

Fig. 15 Optimal design of the energy source hybrid SPV/electric grid system for the master cell (operates 24 h)





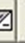











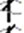




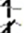








Solar (kWh/m <sup>2</sup> /d)						PV (kW)	L16P	Conv. (kW)	Grid (kW)	Initial Capital	Operating Cost (\$/yr)	Total NPC	COE (\$/kWh)	Ren. Frac.	Batt. Lf. (yr)
5.100						1.2	5	1.0	0.8	\$ 7,200	530	\$ 13,279	0.254	0.41	9.0
5.200						1.2	5	1.0	0.8	\$ 7,200	526	\$ 13,228	0.253	0.42	9.0
5.300						1.2	5	1.0	0.8	\$ 7,200	521	\$ 13,176	0.252	0.42	9.1
5.400						1.2	5	1.0	0.8	\$ 7,200	517	\$ 13,126	0.251	0.43	9.1
5.500						1.0	5	1.0	0.8	\$ 6,400	541	\$ 12,608	0.241	0.39	8.9

Fig. 16 Optimal design of the energy source hybrid SPV/electric grid system for the cell that operates at high traffic only (13 h)

10.2.1 Optimization criteria

Figures 15 and 16 include a summary of the technical and economic criteria for an optimal design of the SPV/electric grid system with different values for the daily radiation for both the cell that operates 24 h, which represents the master cell, and the cell that operates 13 h at high traffic only.

For the first three cases [5.1–5.3 kWh/(m<sup>2</sup> day)] from Fig. 15], the SPV optimal size is the same, 2 kW; the difference is in the energy contribution. The contribution of energy from the solar power system increases with the increase in radiation rate, while the pollution rate decreases. However, with the continuing increase in solar radiation [5.4–5.5 kWh/(m<sup>2</sup> day)] and the electrical grid capacity of 0.8 kW, the optimal size of SPV will be decreased in order to minimize NPC for the solar power system, with guaranteed efficiency of both sustainability and reliability in the system, which is the goal of the HOMER software. The same analysis can be applied to the SPV optimal size in Fig. 16.

System costs consist of (i) initial capital costs paid at the beginning of the project with the largest proportion of costs going to solar cells (approximately \$4/W), (ii) operating costs paid annually, mostly to operate and maintain the electric grid, and (iii) NPC, representing all costs that occur within the project lifetime, including initial capital costs, operation and maintenance cost of components, and replacement costs. More details are provided in the economic analysis in the next subsection.

10.2.2 Energy yield analysis

Figures 17 and 18 summarize the annual energy contribution of the solar electric system and the existing electrical grid for different values of the average daily solar radiation for both the master cell and the cell that operates 13 h at high traffic

only. It is clear that when the solar radiation rate increased, the annual contribution of the solar power system increased at the same SPV size. The instances when the energy purchased from an electrical corporation decreased provide a good indicator of when to decrease the maintenance and operational costs for the EG.

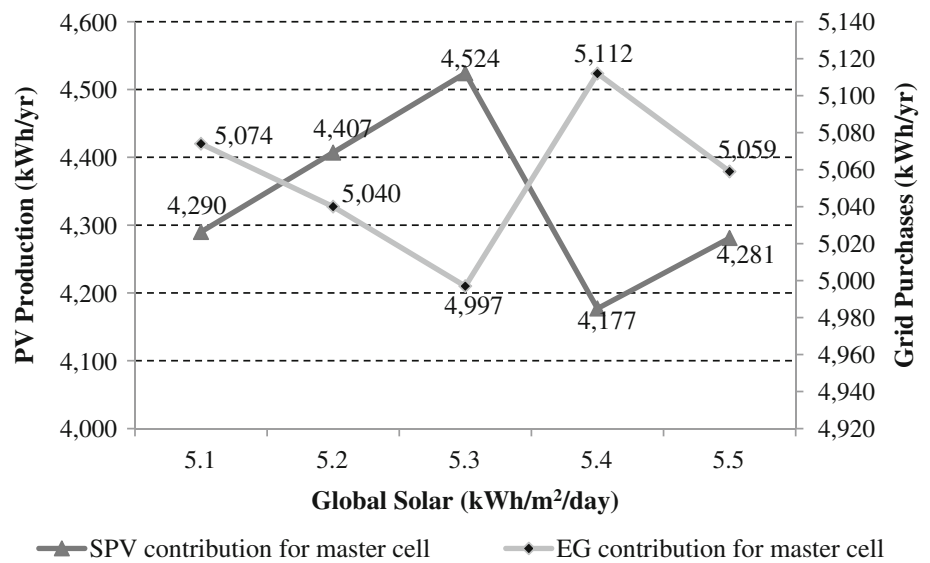
From Fig. 17, in the first three cases [5.1–5.3 kWh/(m<sup>2</sup> day)] where the system has the same size SPV, the solar power system contributes 46, 47, and 48 %, respectively, of the total annual energy needed to supply the BS load. At [5.4–5.5 kWh/(m<sup>2</sup> day)], increases in the rate of radiation at the same condition of a grid purchase with a capacity of 0.8 kW leads to a decrease in the size of SPV, hence decreasing the overall costs with the contribution of energy up to 45 and 46 %. It is clear that the average annual energy consumption of the electrical grid decreased to 45–48 % in the master cell case.

From Fig. 18, in the first four cases [5.1–5.4 kWh/(m<sup>2</sup> day)] where the system has the same size of SPV, the solar power system contributes 49, 50, 51, and 52 % of the total annual energy; the percentage of contributions of the solar power system are high, due to the short duration of the load (10 a.m. to 11 p.m.) and, moreover, mostly occurred during the day when sunlight was available (10 a.m. to 6 p.m.). The average annual energy consumption of the electrical grid decreased to 49–54 %.

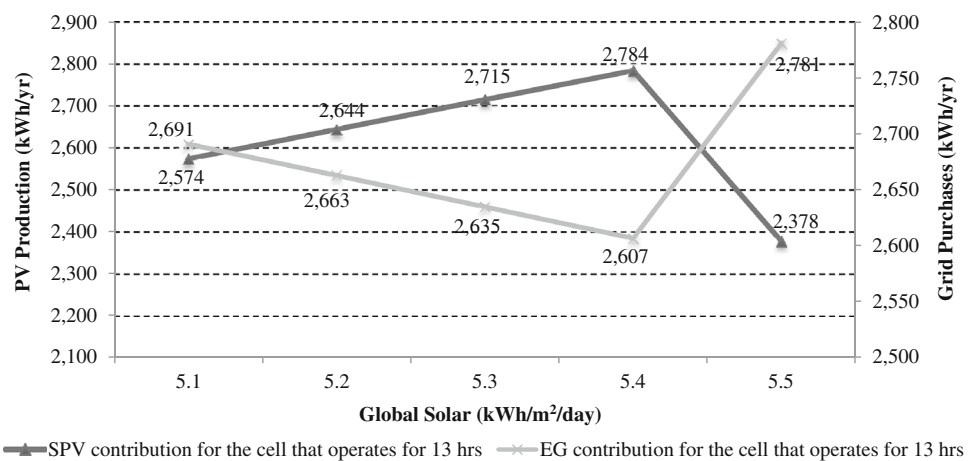
10.2.3 Economic analysis

The costs for both of the two cases are provided in Figs. 15 and 16. In this analysis, Malaysia, with its average daily solar radiation of 5.1 kWh/m<sup>2</sup>, was used as a case study for a master cell design, but the same methodology can be applied to other cases. The total NPC represents all costs that occur within the project lifetime (20 years), including initial capital

**Fig. 17** Annual energy contribution of different sources with different average solar radiation for the master cell



**Fig. 18** Annual energy contribution of different sources with different average solar radiation values for cell operation at high traffic only (13 h)



costs, operation and maintenance cost of components, and replacement costs. From Fig. 15, the total NPC at 5.1 kWh/m<sup>2</sup> is \$23,520; how is this amount distributed over the project’s lifetime? Fig. 19 provides more details.

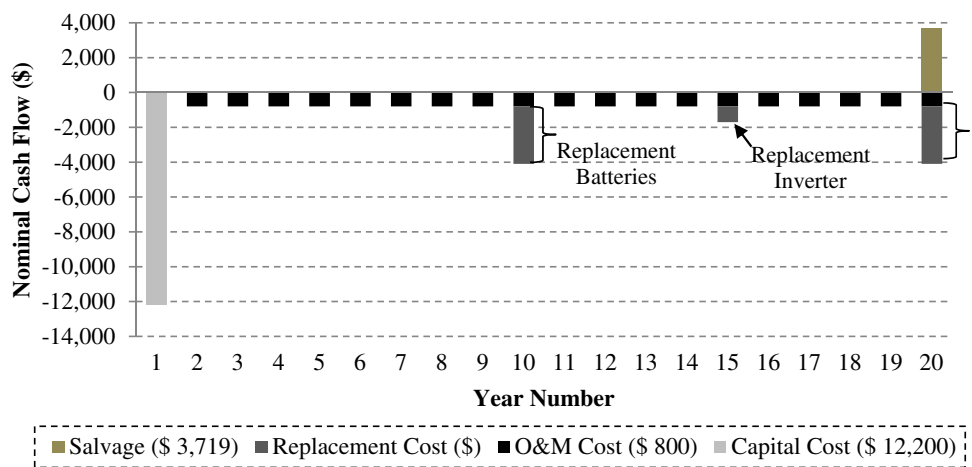
The *initial capital cost* is paid only at the beginning of the project. This cost is directly proportional to the size of the solar power system. Therefore, when the solar radiation rate increases, this leads to a decreased SPV size and initial capital cost, due to the fact that SPV is the most expensive element in the solar power system, as shown above in Figs. 15 and 16. In this study, at 5.1 kWh/(m<sup>2</sup> day), the total initial capital cost is \$12,200, as shown in Fig. 15 above, which breaks down as follows: (i) 65.6 % for the SPV (size 2kW × cost \$4,000/1kW = \$8,000), (ii) 27 % for the battery units (11 units × cost \$300/unit = \$3300), and (iii) 7.4 % for the inverter (size 1 kW × cost \$900/1kW = \$900); the charger controller cost is \$2000. SPV represents the bulk of these costs.

The annual cost for the *maintenance and operation* of the system amounts to \$800, as shown in Fig. 19. The

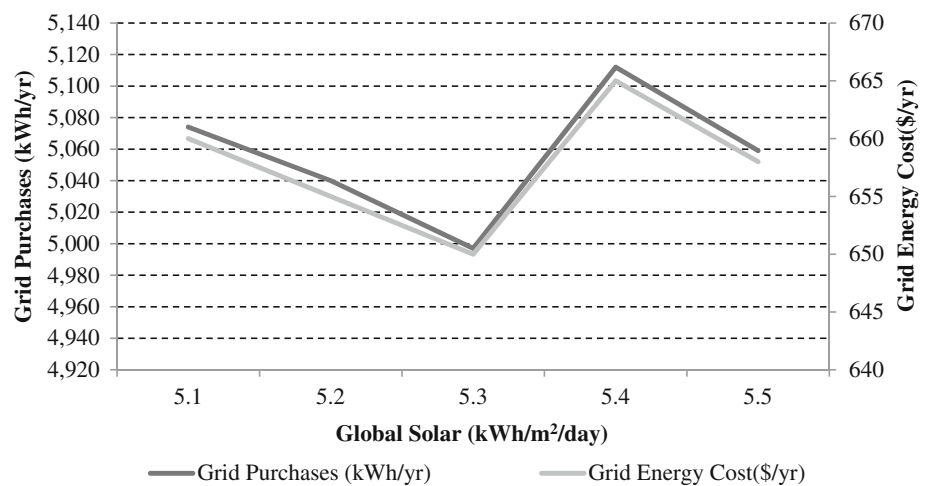
grid represents the bulk of this cost at \$660/year (grid purchases (kWh/year) are shown in Fig. 17 × energy retail price \$0.13/kWh). Thus, the lower energy consumption of the electrical grid and the increased reliance on the solar power system provide more operational expenses, which achieves a greater rate of solar radiation. Figure 20 below describes the comparison between solar radiation, grid purchases, and grid energy cost for a master cell design. As for the other components, the battery, SPV, and inverter costs are \$110, \$20, and \$10/year, respectively.

For *replacement costs*, the batteries represent the bulk, 88 % (11 unit × \$300/unit = 3300 every 10 years, as shown in Fig. 19), as each battery is replaced twice during the project lifetime; this is due to the fact that the number of batteries in the system is large and the operational lifetime is very short compared with the other components. Figure 21 below shows the comparison between solar radiation, number of batteries, and the exact battery lifetime in this study. The inverter is replaced once during the project lifetime (1 kW × \$900 = \$900), and there is no replace-

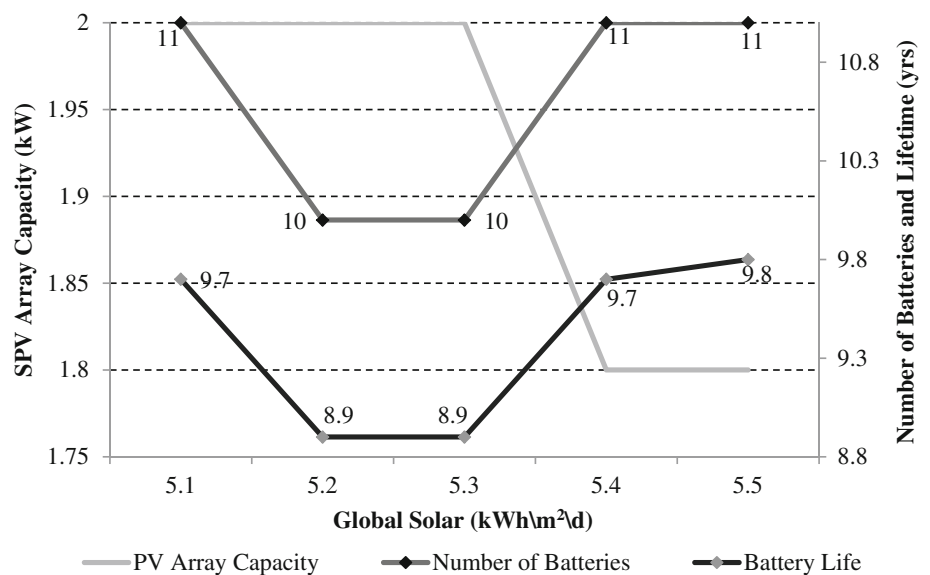
**Fig. 19** Cash flow summary of the SPV/electric grid hybrid power system within the project lifetime at a solar radiation level of 5.1 kWh/(m<sup>2</sup> day)



**Fig. 20** Comparison between solar radiation, grid purchases, and grid energy cost for a master cell design



**Fig. 21** The comparison between solar radiation, number of the batteries, and the exact battery lifetime

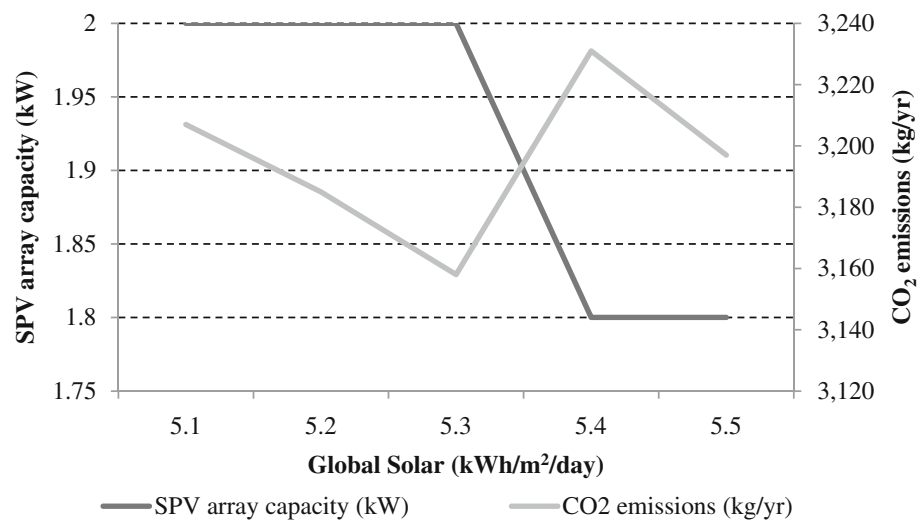


ment cost for the SPV because the project lifetime is equal to the SPV lifetime. Thus, the total replacement cost during the project lifetime is  $2 \times 3,300 + 900 = \$7500/20$  years.

10.2.4 Greenhouse gas (GHG) emissions

Due to improved manufacturing techniques and higher volumes, the carbon footprint of solar panels is now much lower.

**Fig. 22** Comparison between solar radiation, SPV array capacity, and CO<sub>2</sub> emission



In general, when both the solar radiation rate and SPV array capacity are increased, the pollution rate decreases. Figure 22 illustrates the comparison between solar radiation, SPV array capacity, and annual carbon dioxide (CO<sub>2</sub>) emissions for master cell design.

It is clear that when the solar radiation rate increases with the same size of the SPV, the CO<sub>2</sub> emissions will be decreased due to the fact that the contribution of energy from solar cells become higher, while the energy contribution of the grid decreases, as discussed in Sect. 10.2.2.

## 11 Conclusion and remarks

This study examined the feasibility of the integration of a solar power system with the electrical grid to supply BS for on-grid sites during the day in order to minimize the cost of OPEX and carbon emissions and to create a method for switching cells on and off to achieve energy gains at night (during low traffic).

The approach of switching on and off should take into account the cell coverage area. A PSO technique was adopted to maximize coverage due to the increasing coverage size of master cells to provide coverage for cells that are switched off during low-traffic periods. The cells are switched off to achieve energy savings at the network level under the constraints of parameters that affect the cell coverage area: the transmission power of a BS, the total antenna gain, the bandwidth, the signal-to-interference plus noise ratio, and shadow fading. The simulation results show that when the cell coverage area increases, the shadowing increases and the SINR decreases, translating into a minimum amount of received power, which may impact the detected and decoded signals. However, the transmitted power and antenna gain maintain

high coverage at the edge of the cell. This study demonstrated that a daily energy savings of up to 34.77 % can be achieved with guaranteed cell coverage area.

In the section on using solar energy for cellular base stations to reduce network operating expenses, three key aspects were investigated: (i) energy yield analysis, (ii) economic analysis, and (iii) greenhouse gas emissions, which can be summarized as follows. When there are increases in both the solar radiation rate and the size of the solar cell, the energy produced from the solar power system will be increased with a positive effect on pollution reduction. Meanwhile, the costs of the system should be taken into account, as the costs will increase with the increase in the size of the solar power system and as the price of solar cells is high. Therefore, this study examined the balance between the size of the solar system, grid purchase capacity, energy purchased, and system costs in order to minimize NPC for the solar power system, with guaranteed efficiency, sustainability and reliability in the system and the goal of using the HOMER software. The study also highlighted that the average daily solar radiation for Malaysia is 5.1 kWh/m<sup>2</sup>. The results show that 48 % of the annual OPEX can be saved.

**Acknowledgments** The authors would like to thank the Universiti Kebangsaan Malaysia for the financial support of this work, under the Grant Ref: ETP-2013-072.

## References

- Ericsson Corporation. (2013). Ericsson Corporation report. Ericsson Mobility Report on the Pulse of the Networked Society. Retrieved August 01, 2014 from <http://www.ericsson.com/res/docs/2013/ericsson-mobility-report-june-2013.pdf>.
- Chen, T., Yang, Y., Zhang, H., Kim, H., & Horneman, K. (2011). Network energy saving technologies for green wireless access networks. *IEEE Wireless Communications*, 18(2), 30–38.



3. Suarez, L., Nuaymi, L., & Bonnin, J.-M. (2012). An overview and classification of research approaches in green wireless networks. *EURASIP Journal on Wireless Communications and Networking*, 2012(1), 1–18.
4. Alsharif, M., Nordin, R., & Ismail, M. (2014). Classification, recent advances and research challenges in energy efficient cellular networks. *Wireless Personal Communications*, 77(2), 1249–1269.
5. Oh, E., Krishnamachari, B., Liu, X., & Niu, Z. (2011). Toward dynamic energy-efficient operation of cellular network infrastructure. *IEEE Communications Magazine*, 49(6), 56–61.
6. Chiaraviglio, L., Ciullo, D., Meo, M., & Marsan, M. (2008). Energy-aware UMTS access networks. In *Proceedings of 11th International Symposium on Wireless Personal Multimedia Communications (WPMC'08)* (pp. 1–5).
7. Chiaraviglio, L., Ciullo, D., Meo, M., & Marsan, M. (2009). Energy-efficient management of UMTS access networks. In *Proceedings of 21st International Teletraffic Congress (ITC 2009)* (pp. 1–8), Paris, September 2009.
8. Marsan, M., Chiaraviglio, L., Ciullo, D., & Meo, M. (2009). Optimal energy savings in cellular access networks. In *Proceedings of IEEE International Conference on Communications Workshops (ICC Workshops)* (pp. 1–5), Germany, June 2009.
9. Zhou, S., Gong, J., Yang, Z., Niu, Z., & Yang, P. (2009). Green mobile access network with dynamic base station energy saving. In *Proceedings of ACMMobiCom'09* (pp. 1–3), Beijing, China, September 2009.
10. Gong, J., Zhou, S., Niu, Z., & Yang, P. (2010). Traffic-aware base station sleeping in dense cellular networks. In *Proceedings of 18th International Workshop on Quality of Service (IWQoS)* (pp. 1–2), 2010.
11. Xiang, L., Pantisano, F., Verdone, R., Ge, X., & Chen, M. (2011). Adaptive traffic load-balancing for green cellular networks. In *Proceedings of 22nd IEEE International Conference on Personal Indoor and Mobile Radio Communications (PIMRC)* (pp. 41–45), Toronto, September 2011.
12. Lorincz, J., Capone, A., & Begusic, D. (2012). Impact of service rates and base station switching granularity on energy consumption of cellular networks. *EURASIP Journal on Wireless Communications and Networking*, 2012(1), 1–24.
13. Bousia, A., Antonopoulos, A., Alonso, L., Verikoukis, C. (2012). Green Distance-Aware Base Station Sleeping Algorithm in LTE-Advanced. In *Proceedings of IEEE International Conference on Communications (ICC)* (pp. 1347–1351), Ottawa, June 2012.
14. Niu, Z., Wu, Y., Gong, J., & Yang, Z. (2010). Cell zooming for cost-efficient green cellular networks. *IEEE Communications Magazine*, 48(11), 74–79.
15. Bhaumik, S., Narlikar, G., Chattopadhyay, S., & Kanugovi, S. (2010). Breathe to stay cool: adjusting cell sizes to reduce energy consumption. In *Proceedings of ACM SIGCOMM workshop on Green networking* (pp. 1–5).
16. Kokkinogenis, S., & Koutitas, G. (2012). Dynamic and static base station management schemes for cellular networks. In *Proceedings of 2012 IEEE International Conference on Global Communications (GLOBECOM)* (pp. 3443–3448).
17. Sthitaprajna Rath, S. M., Ali, Md, & Iqbal, N. (2012). Strategic approach of hybrid solar-wind power for remote telecommunication sites in India. *International Journal of Scientific & Engineering Research*, 3(6), 1–6.
18. Pragya, N., Nema, R. K., & Saroj, R. (2010). Minimization of green house gases emission by using hybrid energy system for telephony base station site application. *Renewable and Sustainable Energy Reviews*, 14, 1635–1639.
19. Ani, V. A., & Emetu, A. N. (2013). Simulation and optimization of hybrid diesel power generation system for GSM base station site in Nigeria. *Electronic Journal of Energy & Environment*, 1(1), 1–20.
20. Martínez-Díaz, M., Villafáfila-Robles, R., & Montesinos-Miracle, D. (2013). Study of optimization design criteria for stand-alone hybrid renewable power systems. In *Proceedings of International Conference on Renewable Energies and Power Quality (ICREPQ'13)* (pp. 20–22), Bilbao, Spain.
21. Subodh, P., Madhu, S. D., Muna, A., & Jagan, N. S. (2013). Technical and economic assessment of renewable energy sources for telecom application: a case study of Nepal telecom. In *Proceedings of 5th International Conference on Power and Energy Systems* (pp. 28–30) Kathmandu, Nepal.
22. Kanzumba, K., & Herman, J. V. (2013). Hybrid renewable power systems for mobile telephony base stations in developing countries. *Renewable Energy*, 51(2013), 419–425.
23. Prabodh, B., Prakshan, N. P., Kishore, N. K. (2009). Renewable hybrid stand-alone telecom power system modeling and analysis. In *Proceedings of TENCON 2009, Singapore* (pp. 1–6).
24. Vincent, A., & Anthony, N. (2013). Potentials of optimized hybrid system in powering off-grid macro base transmitter station site. *International Journal of Renewable Energy Research*, 3(4), 1–11.
25. Auer, G., Blume, O., Giannini, V., Godor, I., Imran, A. M., Jading, Y., et al. (2010). Energy efficiency analysis of the reference systems, areas of improvements and target breakdown. *EARTH Project Report, Deliverable, D2(3)*, 1–68.
26. Johansson, K., Furuskar, A., Karlsson, P., Zander, J. (2004). Relation between base station characteristics and cost structure in cellular systems. In *Proceedings of 15th IEEE International Symposium on Personal, Indoor and Mobile Radio Communications (PIMRC 2004)* (pp. 2627–2631).
27. Debus, W. (2006). *RF path loss & transmission distance calculations*. New York: Axonn, LLC.
28. Sesia, S., Toufik, I., & Baker, M. (2011). *LTE - The UMTS long term evolution: From theory to practice* (2nd ed.). New York: Wiley.
29. Goldsmith, A. (2005). *Wireless Communication* (2nd ed.). Cambridge: Cambridge University Press.
30. Kennedy, J., & Eberhart, R. (1995). Particle swarm optimization. In *Proceedings of IEEE International Conference on Neural Networks* (pp. 1942–1948).
31. Mekhilefa, S., Safaria, A., Mustaffaa, W. E. S., Saidurb, R., Omara, R., & Younisc, M. A. A. (2012). Solar energy in Malaysia: Current state and prospects. *Renewable and Sustainable Energy Reviews*, 16(1), 386–396.
32. Borhanazada, H., Mekhilefa, S., Saidurb, R., & Boroumandjazib, G. (2013). Potential application of renewable energy for rural electrification in Malaysia. *Renewable Energy*, 59(2013), 210–219.
33. Sopian, K., Hj, M. Y., & Othman, A. W. (1995). The wind energy potential of Malaysia. *Renewable Energy*, 6(8), 1005–1016.
34. Borhanazada, H., Mekhilefa, S., Saidurb, R., & Ganapathy, V. G. (2014). Long-term wind speed forecasting and general pattern recognition using neural networks. *IEEE Transactions on Sustainable Energy*, 5(2), 546–553.
35. Azhari, A. W., Sopian, K., Zaharim, A., & Al ghou, M. (2008). A new approach for predicting solar radiation in tropical environment using satellite images e case study of Malaysia. *WSEAS Transactions on Environment and Development*, 4(4), 2008.
36. Khatib, T., Mohamed, A., Sopian, K., & Mahmoud, M. (2012). Solar energy prediction for Malaysia using artificial neural networks. *International Journal of Photoenergy*, 2012, 1–16.
37. Gunter, S. (2009). The green base station. In *Proceedings of 4th International Conference on Telecommunication - Energy Special Conference (TELESCON)* (pp. 1–6).
38. Rehman, S., & Al-Hadhrani, L. M. (2010). Study of a solar PVdieselebattery hybrid power system for a remotely located population near Rafha, Saudi Arabia. *Energy*, 35(12), 4986–4995.
39. Lambert, T., Gilman, P., & Lilienthal, P. (2014). Micropower System Modeling with HOMER (2006). Retrieved

August 01, 2014 from <http://homerenergy.com/documents/MicropowerSystemModelingWithHOMER.pdf>.

40. Malaysian Energy Corporation. (2014). Retrieved August 01, 2014 from <http://www.tnb.com.my/business/for-industrial/pricing-tariff.html>.



**Mohammed H. Alsharif** received his engineering degree in Communication and Control from the Electrical and Computer Engineering Department at the Islamic University of Gaza (IUG), Palestine, in 2008 and an M.S. degree in Computer and Communication Engineering from Universiti Kebangsaan Malaysia (UKM), Malaysia, in 2012. Alsharif is currently pursuing a Ph.D. degree in Electrical and Electronic Engineering at the Universiti Kebangsaan

Malaysia. His research interests include wireless communications, green communication, cooperative communication, and multiple radio access technologies.



**Rosdiadee Nordin** received a B.Eng. degree in electrical, electronic and systems engineering from Universiti Kebangsaan Malaysia in 2001 and a Ph.D. degree in wireless engineering from the University of Bristol, United Kingdom in 2011. From 2002 to 2006, he was a telecommunication engineer with the Maxis Communications in Malaysia. His research interest includes energy efficient wireless communications, resource allocation, advanced Multiple-Input

Multiple-Output (MIMO) techniques, fundamental study of TV White Spaces (TVWS) and indoor wireless localization. Dr. Nordin is a professional engineer with the Board of Engineers Malaysia (BEM), corporate member for Institute of Engineer Malaysia (IEM) and member of The Institute of Electronics, Information and Communication Engineers (IEICE), Japan. He is a senior member of IEEE and serves as a reviewer in some IEEE journals related to wireless communications. In addition, he has been appointed to technical committees in several IEEE Malaysia-sponsored conferences.



**Mahamod Ismail** joined the Department of Electrical, Electronics and System Engineering, Faculty of Engineering and Built Environment, University Kebangsaan Malaysia (UKM) in 1985. He is currently a Professor in Communication Engineering. He received a B.Sc. degree in Electrical and Electronics from University of Strathclyde, U.K. in 1985, an M.Sc. degree in Communication Engineering and Digital Electronics from University of Manchester

Institute of Science and Technology (UMIST), Manchester U.K. in 1987, and a Ph.D. from University of Bradford, U.K. in 1996. He was with the first Malaysia Microsatellite TiungSat Team Engineers in Surrey Satellite Technology Ltd. U.K. from June 1997 until March 1998. In the summer semester of 2003, he served as a Guest Professor in Computer Engineering in the University of Duisburg-Essen, Duisburg Germany funded by the German Academic Exchange Services (DAAD). His research interests include mobile and satellite communication, and wireless networking, particularly focusing on radio resource management for next-generation wireless communication networks. He is a Senior Member of IEEE USA and was the chair of IEEE Malaysia Section from 2011 to 2013.